NUMERICAL INTERPRETATION OF FULLY BIO-RESORBABLE GLASS FIBRE REINFORCED COMPOSITES

Xi Gao[1], Menghao Chen[2], Xiaogang Yang[1], Lee T. Harper[2], Ifty Ahmed[2], Jiawa Lu[1]

[1] Faculty of Science and Engineering, University of Nottingham Ningbo China, 315100, China, xi.gao@nottingham.edu.cn

[2]Faculty of Engineering, University of Nottingham, NG7 2RD, United Kingdom, menghao.chen@nottingham.ac.uk

Keywords: Bio-resorbable composites, Finite element method, Elastic property, Cohesive elements, Interfacial stiffness.

ABSTRACT

The improvement of in-situ polymerization (ISP) over laminate stacking (LS) was highlighted in a recent publication and studied in this work via 3D finite element model. It was assumed that the fibre/matrix interface was a cohesive layer and cohesive elements were adopted to model the interface. Elastic stiffness was determined by using an inverse method based on the experimental data. In addition to the interface, the effects of void ratio and misalignment were investigated and these influences were quantitatively integrated into the interfacial stiffness. Comparisons against experimental results revealed that the numerical model was capable of modelling the difference in the interface of the composites produced by the different manufacturing methods, e.g. the numerical prediction of the stiffness of the composites with 35% fibre volume fraction was ~8.5GPa while the experimental data was ~9GPa. When the fibre volume fraction was 50%, the numerical prediction was ~20GPa compared with ~18GPa from experimental data. Moreover, the potential of the numerical model to detect failure is also discussed.

1 INTRODUCTION

Traditionally, load-bearing metal implants have been used in surgical procedures for bone fixation purposes. However, these implants are associated with 'stress shielding', which weakens the surrounding bone and increases re-fracture risk after device removal [1-4]. There has been a strong interest in developing fully bio-resorbable polymers as bone fracture fixation devices such as plates, screws, pins and rods. However, the limitation for these polymers is insufficient mechanical properties for weight bearing applications [5, 6]. The ideal replacement of traditional smetal bone fixation devices should have excellent biocompatibility, be fully bio-resorbable, have sufficient initial mechanical properties to support bone healing during the initial stages, and then would gradually degrade in order to transfer stress to the healing bone [4, 7]. A lot of works have been made to introduce fully resorbable fibre as the reinforcement to enhance the bio-resorbable polymer. Possibility of natural fibres have also been excluded due to the dimensional instability and unavoidable variable properties caused by short fibre limitation [8, 9]. Phosphate glass fibre (PGF) has been regarded as the desirable reinforcement because it has high modulus, is easy to control the length and is fully bio-resorbable [10, 11].

In the manufacturing of PGF reinforced composites, achieving satisfactory adhesion between the fibre and the matrix has been one of the challenges. The most frequently adopted manufacturing methods for this kind of composites are laminate stacking (LS) and hot press moulding [12-14]. However, due to the degradation of the interface, the rapid loss in mechanical properties of the composites manufactured by LS after immersion in aqueous environment has

been reported by several studies [15, 16]. The rapid hydrolysis of the interface results in failure of effective stress transfer between the fibre and the matrix [17]. An alternative manufacturing method referred to as in-situ polymerization (ISP) was adopted to overcome the shortcomings of LS process [7]. As suggested by the name of the method, the matrix is formed directly around the fibres in a mould by injecting in-situ polymerized reaction mixture. The advantage of ISP over LS is that ISP process facilitates better impregnation of the fibre, and thus provides significantly enhanced mechanical properties, which is believed to be due to the enhanced interface. The flexural modulus of the composites with 35% fibre volume fraction manufactured by ISP was ~15GPa, while it was ~9GPa for those produced by LS. In addition, composites produced by ISP showed improved resistance to aqueous environment than those by LS. After 28-day degradation test, the flexural modulus of composites with 35% fibre volume fraction by ISP and LS reduced to ~6GPa and ~0.7GPa, respectively [7].

The interface between the fibre and the matrix has been shown to have great influence on the composites mechanical properties. A number of studies have been reported investigating the interfacial properties of fibre reinforced composites [18, 19]. The most frequently used method is the single fibre pull-out test [20], which calculates the interfacial properties by establishing the load against extension. Recently, fibre fragmentation and photoelasticity were combined to evaluate the interfacial strength, which required single fibre crack from the fibre fragmentation test [21]. It was found that the normalized interfacial strength and the characteristic length, which is defined as the subtraction of the distance of the farthest point of the shear traction contour in the matrix and the fibre radius, have a linear relationship, therefore the interfacial strength could be determined once the characteristic length is found out by the photoelastic analysis. In addition to the experimental tests, numerical methods, such as the finite element (FEM) analysis, have been adopted to investigate the fibre/matrix interface of fibre reinforced composites. The interface was modelled as a thin layer enclosing the short fibre, and the interfacial bond was represented by the mechanical properties of the cohesive layer, which was defined to be of thickness of $0.025d$ with d be the diameter of the fibre [19]. The results showed that the tensile elastic moduli of the composites were influenced by the interfacial bond and the orientation of the fibres; the elastic moduli decreased with increasing fibres orientation angle, and increased with better interfacial bond [19]. More recently, Soni et al [22] studied the influence of the fibre/matrix interface on the global material response by developing a multi-fibre multi-layer micromechanical finite element model. They found that higher values of interface stiffness and interface cohesive strength led to higher value of shear stress predictions, and the axial response of the composites was stiffer than the transverse response. In another FE analysis study, Maligno et al assumed the fibre/matrix interface to be a perfect bond to investigate the effect of residual stress due to the curing process on damage evolution in unidirectional (UD) fibre reinforced composites [23]. It was shown that due to the assumption of perfect bonding between the fibre and the matrix, the energy based failure criteria is particular sensitive to high triaxial stresses which arise at the fibre/matrix interface on uniaxial tensile loading. In above studies, the FE analysis has been shown to be capable of generating reasonable solutions in these simulations, though some simplified assumptions, e.g. uniform boundary conditions, isotropic materials, etc., were made in the models.

In this study, FE analysis was adopted to carry out comprehensive investigations on the mechanical properties of fully bio-resorbable PGF reinforced composites considering the influence of the firbe/matrix interface. The interface was assumed to be a cohesive layer with finite thickness ($0.0002d$, where d is the diameter of the fibre) and was represented by cohesive elements with continuous response. The experimental data of composites manufactured by LS and ISP were employed to determine the interfacial properties by the inverse method, and numerical modelling was adopted to verify the calibration. The composites were modelled as the periodic representative volume elements (RVE), the use of which has been well established [23, 24]. The RVE used in this work was based on a 3D model with square array of the fibre as can be seen in Figure 1. Three different fibre volume fraction (V_f) RVEs were investigated, and the dimension of the RVEs were determined based on the fibre

diameter and V_f . Moreover, in order to fully understand the difference between the interface of the composites manufactured by LS and ISP, the void ratio of the samples was examined and integrated quantitatively into the definition of the interfacial stiffness.

2 METHODOLOGY

2.1 Finite element geometry

FEM was adopted to model the performance of the composites on micro-mechanical level. In order to reduce computation cost, the composites were represented by a unit cell model due to its periodicity as shown in Fig. 1. The unit cell model was a representative of the mechanical behaviour of the whole specimen. In this FE model, the fibre and the matrix were assigned with different isotropic elastic properties and positioned concentrically. The interface between the fibre and the matrix was modelled as a cohesive zone and represented by a finite thick layer of cohesive elements. The model was treated as an axial symmetrical problem, which assumed that the fibre was a perfect cylinder of length l, and radius r in the middle of a cube of matrix. The fibre employed in previous experimental work was about of 0.1mm in radius for various fibre volume fractions [7], therefore, the dimensions of the matrix cube were decided based on the fibre radius, i.e. 0.4mm, 0.35mm and 0.25mm for fibre volume fractions of 20%, 35% and 50%, respectively. The commercial FE software ABAQUS was employed to build this FE model and carry out the numerical simulations. The fibre and the matrix were meshed with the 3D linear wedge elements with full integration (C3D6) and the interface was meshed with the 3D cohesive hexagonal elements with full integration (COH3D8). Two key aspects in this FE model were: the boundary conditions set up to load the model as it was in real mechanical situation; the interfacial properties set up to bond the fibre and the matrix properly.

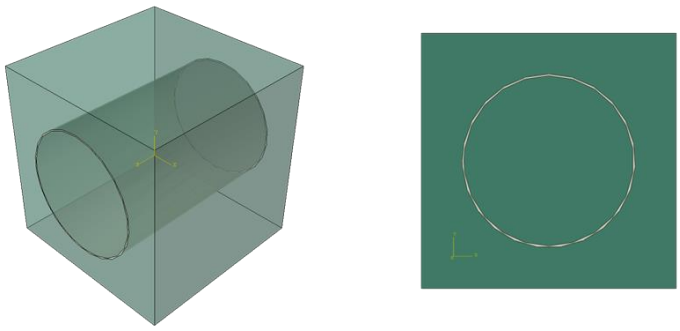

Figure 1 Illustration of the FE model of containing single fibre

2.2 Governing equations and boundary conditions

In general, the composites reinforced with parallel aligned continuous long fibres exhibit orthotropic material properties. The composites modelled in this paper were assumed to be transversely isotropic, which means the mechanical properties are symmetrical about the fibre direction. For transversely isotropic material, the elastic relation can be described by

$$\begin{Bmatrix} \bar{\sigma}_1 \\ \bar{\sigma}_2 \\ \bar{\sigma}_3 \\ \bar{\sigma}_4 \\ \bar{\sigma}_5 \\ \bar{\sigma}_6 \end{Bmatrix} = \begin{bmatrix} C_{11} & C_{12} & C_{12} & 0 & 0 & 0 \\ C_{12} & C_{22} & C_{23} & 0 & 0 & 0 \\ C_{12} & C_{23} & C_{22} & 0 & 0 & 0 \\ 0 & 0 & 0 & (C_{22}-C_{23})/2 & 0 & 0 \\ 0 & 0 & 0 & 0 & C_{66} & 0 \\ 0 & 0 & 0 & 0 & 0 & C_{66} \end{bmatrix} \begin{Bmatrix} \bar{\varepsilon}_1 \\ \bar{\varepsilon}_2 \\ \bar{\varepsilon}_3 \\ \bar{\gamma}_4 \\ \bar{\gamma}_5 \\ \bar{\gamma}_6 \end{Bmatrix} \tag{1}$$

where $\boldsymbol{\sigma}, \boldsymbol{\varepsilon}, \boldsymbol{\gamma}$ and $\mathbf{C}$ represent the stress, the normal strain, the shear strain and the stiffness tensor, respectively; the 1-direction is aligned with the fibre direction, 2- and 3-direction are the other two orthogonal directions. The over-bar indicates the average value calculated over the volume of the RVE. Once the entries of the stiffness tensor matrix are known, the elastic properties of the composites can be computed as follows:

$$\begin{aligned} E_1 &= C_{11} - 2C_{12}^2 / (C_{22} + C_{23}) \\ \nu_{12} &= C_{12} / (C_{22} + C_{23}) \\ E_2 &= \left[C_{11}(C_{22} + C_{23}) - 2C_{12}^2 \right](C_{22} - C_{23}) / \left(C_{11}C_{22} - C_{12}^2 \right) \\ \nu_{23} &= \left(C_{11}C_{23} - C_{12}^2 \right) / \left(C_{11}C_{22} - C_{12}^2 \right) \\ G_{12} &= C_{66} \end{aligned} \tag{2}$$

where E, ν and G stands for the elastic modulus, the Poisson ratio and the shear modulus, respectively. In order to compute the overall elastic stiffness matrix in Eq.(1), a series of boundary conditions are applied. One usual boundary condition is to apply uniform strain in normal direction of the RVE and constrain the displacement in other two directions [25-27]. Assumption made in the application of this kind of boundary condition is that the fibre and the matrix are in perfect bonding. It has been shown that the boundary condition of uniform strain is reasonable in numerical studies, whose focus is not the influence of the interface. Whereas the aim of this paper is to investigate the mechanism of the influence of the interface, a uniform stress was applied as boundary condition. Unlike the uniform strain which assumes perfect bonding, the uniform stress allows relative displacement of the fibre and the matrix such that the influence of the interface can be detected. The boundary conditions were applied as follows:

$$\begin{aligned} &\sigma(x, y, a) = T; \\ &u(x, y, 0) = 0; \\ &u_1(0, y, z) = u_1(a, y, z) = 0; \\ &u_{r2}(0, y, z) = u_{r2}(a, y, z) = 0; \\ &u_{r3}(0, y, z) = u_{r3}(a, y, z) = 0; \\ &u_2(x, 0, z) = u_2(x, a, z) = 0; \\ &u_{r1}(x, 0, z) = u_{r1}(x, a, z) = 0; \\ &u_{r3}(x, 0, z) = u_{r3}(x, a, z) = 0. \end{aligned} \tag{3}$$

in which z represents the axial direction, while x and y represent the other two orthogonal directions, the subscript $r1, r2$ and $r3$ mean the rotation about the axis 1, 2, and 3; a is the length of the RVE; T is the uniform tensile stress applied on the boundary and equals $10Mpa$ if not specified. The application of the boundary condition results in complex stress and strain state inside the RVE. The calculation of the average stress and strain over the volume of the RVE involves the homogenization of the stress-strain relation of all the elements. Due to the assumption of the cohesive interface and that the cohesive elements do not provide any off-thickness stress [28]; the direct contribution to the average stress and strain from the cohesive elements should be subtracted from the entire volume. Therefore, the modified homogenization algorithm is written as the following equations:

$$\bar{\varepsilon}_i = \frac{1}{V}\int_V \varepsilon_i(x, y, z)dV - \frac{1}{V^c}\int_V \varepsilon_i^c(x, y, z)dV^c \tag{4}$$

$$\bar{\sigma}_i = \frac{1}{V}\int_V \sigma_i(x, y, z)dV - \frac{1}{V^c}\int_V \sigma_i^c(x, y, z)dV^c \tag{5}$$

where V is the total volume and the superscript c stands for the cohesive element. The detection and subtraction of the contribution from cohesive elements are realized by the Python post

processor. Once the average stress and strain are evaluated, the elastic stiffness tensor can be obtained through the equation below:

$$C_{ij} = \frac{\bar{\sigma}_j}{\bar{\varepsilon}_j} \tag{6}$$

Theoretically, in ideal assumption, the elastic modulus of the composites can be determined by the Rule of Mixture (ROM) as follows:

$$E_c = E_f V_f + E_m (1 - V_f) \tag{7}$$

in which E stands for the elastic moduli, the subscripts c, f and m stand for the composite, fibre and the matrix, respectively, V_f stands for the fibre volume fraction. One key assumption of Eq. (7) is that the interface between the fibre and the matrix is perfect, which is against the assumption in this paper. However, the elastic modulus calculated by the ROM can be adopted as the upper limit reference for the numerical predictions.

2.3 Model constants determination

In this FE model, the fibre/matrix interface was represented by a cohesive zone between the fibre and the matrix, whose property is vital to the overall elastic modulus of the composites. In reality, the interfacial properties can be influenced by material types and manufacturing methods [18, 29]. The mechanical properties of the interface can be experimentally tested by the single fibre pull out test [30]; however, limited data are available for various material types of the fibre and the matrix, and for the different manufacturing methods. Therefore, an inverse method was applied to determine the interfacial stiffness. Across different material types and manufacturing methods, one common issue weakening the interface is the voids existing in the interface area [26, 31]. The properties of the interface used in the simulations in this paper were determined by taking into account the effect of void ratio.

Theoretically, the elastic modulus of the composites increases with higher fibre volume fraction because the fibre is implemented as the reinforcement. However, practically, this is not always the case as the higher fibre volume fraction may result in dry bundles of fibres due to the manufacturing limitation as can be seen in Fig. 2. These dry bundles hardly have effective bonding among them and exert an adverse effect on the elastic modulus of the composites since these fibres would slip easily under loading. This issue can be reduced by improving the manufacturing method. In the following sections, the performance of the composites manufactured from two methods, LS and ISP, were compared. The significant differences in samples with 50% fibre volume fraction are discussed.

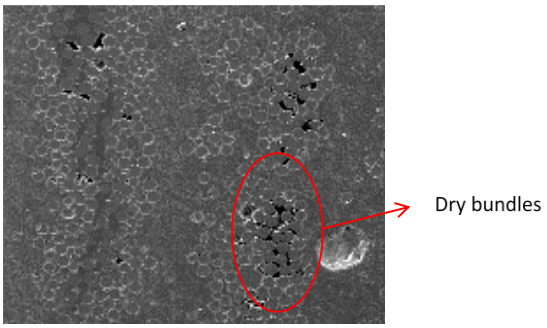

Figure 2 Illustration of dry bundle of fibres occur in composites of 35% volume fraction manufactured by LS method

3 RESULTS AND DISCUSSIONS

3.1 Material constants determination

3.1.1 Void ratio

The samples were 40mm in the total length, and there were 8 locations with a uniform interval along the axial direction selected to take SEM at the cross-section. Once the SEM images were taken, the void ratio was obtained by the image processing technique. Fig. 3 shows the SEM images at one location of the composites by ISP with the fibre volume fraction of 20%. The voids, which are in black in Fig. 3(a), were marked in red in the processed SEM as shown in Fig. 3(b). The void ratio at this location was evaluated by calculating the percentage of the red pixels over the whole pixels. The overall void ratio of the composites was obtained by taking the average of the void ratios at all the locations.

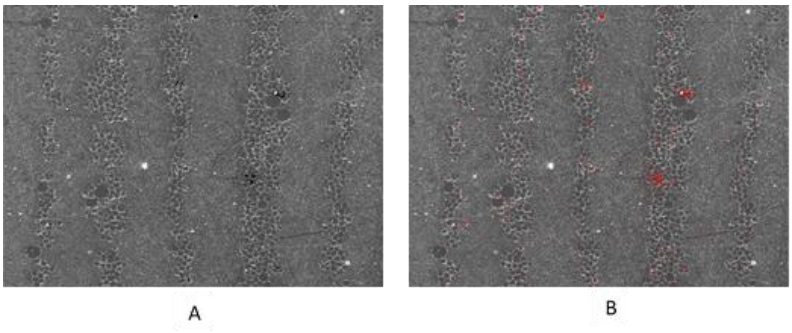

Figure 3 SEM of one cross section for Vf=20% (A) original SEM; (B) processed SEM

The void ratios obtained through this method are listed in Table 1. Overall, the void ratio of the composites by LS was higher than those by ISP for each fibre volume fraction, which was consistent with the fact that ISP generates better impregnation and wet-out of fibre than LS. A clear decline of void ratio with increasing fibre volume fraction was observed for composites manufactured via the ISP process, which indicated that the composites elastic modulus increased steadily. However, the composites manufactured via LS process showed a descending trend for the volume fractions of 20% and 35%, whereas for the volume fraction of 50%, the void ratio was 2.527%. The increase for LS composites was suggested to be caused by the occurrence of dry bundle of fibres for high fibre volume fraction, which in return jeopardized the mechanical properties of the composites. Consequently, the difference between the elastic modulus of LS and ISP composites became more significant at high fibre volume fraction, which was consistent with the experimental data and the numerical predictions in the following sections.

Volume fraction	LS	ISP
20%	1.783%	0.255%
35%	1.422%	0.214%
50%	2.527%	0.181%

Table 1 Void ratio of composites by two manufacturing methods with different fibre volume fractions

3.1.2 Interfacial stiffness determination

Having analysed the void ratio of the composites, the numerical simulation is conducted in this section. In order to verify the numerical model, the numerical predictions are compared with the experimental data and the theoretical values obtained by ROM. The material properties and the model parameters adopted are tabulated in Table.2. It should be noted that the stiffness of the interface is essential to assure proper bonding between the fibre and the matrix. The interfacial stiffness in the FE model in this work is proposed to be determined by Eq. (10):

$$E_i = E_{ref} * \left(1 - V_{void}\right)^2 \tag{8}$$

where $\boldsymbol{E_i}$ stands for the interfacial modulus, $\boldsymbol{V_{void}}$ stands for the void ratio as shown in Table 1, $\boldsymbol{E_{ref}}$ stands for the reference modulus. The value of $\boldsymbol{E_{ref}}$ was determined inversely by testing various values of $\boldsymbol{E_{ref}}$ to fit the numerical prediction with the experimental data of the composites, with 35% fibre volume fraction by LS. Herein the value of $\boldsymbol{E_{ref}}$ was set as 30GPa, unless specified.

	Fibre	**Matrix**	**Interface**
Young's modulus	42.4Gpa	0.19Gpa	$E_{ref}*(1-V_{void})^2$ Gpa
Poisson's ratio	0.3	0.3	0.3
Isotropic?	Yes	Yes	Yes
Material type	Homogeneous solid	Homogeneous solid	Cohesive with continuous response
Element type	C3D6	C3D6	COH3D8

Table 2 Material properties and parameters adopted in numerical modelling

Fig. 4 illustrates the comparisons of the FE predictions and the experimental data of LS and ISP composites, with different fibre volume fractions. It can be seen that the FE predictions for the composites with fibre volume fraction of 20% and 35% agree well with the experimental data, however, for the composites with the volume fraction of 50% the FE prediction is much higher than the LS data but close to the ISP data and the ROM evaluation. This is because the dry bundle of fibres generated from LS manufacturing process weakens the composites due to the poor interface among dry bundles, while the ISP method produced a better impregnation and wet-out of fibres thus the composites modulus was higher at 50%. In the FE models the fibres were positioned with uniform interface between each other, therefore, the FE prediction was close to the ISP data. The results in Fig. 4 displays the capability of the FE model to generate reasonable predictions comparing with the experimental data, though the LS data at 50% volume fraction needs more conditions to define the manufacturing deficiency.

3.2 Variation of interfacial stiffness

The reference value of the interfacial stiffness has been set as 30GPa, though the effect of variation of interfacial stiffness is studied. As the interface was modelled as a cohesive layer, it is expected that with higher interfacial stiffness leads to stiffer elastic response. Fig. 5 shows the strain contour at the loading end of the FE model. It can be seen that the strain of the fibre and the matrix are different under the same load, which means that with the application of the boundary conditions and the assumption of cohesive interface, relative displacement between the fibre and the matrix can be detected. The strain of the fibre is uniform at rather insignificant level since the fibre is defined as a stiff material. In contrast, the strain of the matrix is more significant. The area of the matrix close to the interface experiences small normal deformation

because the cohesive interface acts as resistance to prevent the matrix from extending. As it becomes distant away from the interface, the effect of the resistance declines, therefore, the strain increases gradually.

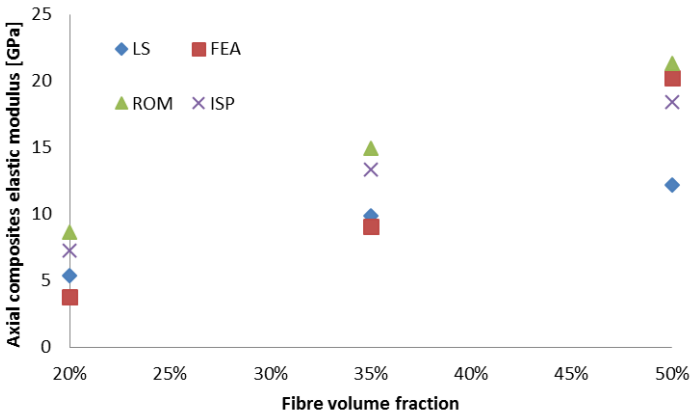

Figure 4 Comparisons of axial elastic moduli of composites predicted by FE model, experimental data and theoretical prediction.

The effect of the cohesive interface can be further observed from Fig. 6. The stiffness of the composites with different fibre volume fractions are plotted against the interfacial stiffness. Overall, the composites stiffness increases with the growth of the interfacial stiffness, which means the composites displays stiffer elastic response with stronger interface. The predictions are in consistency with the expectation. The cohesive interface acts as the shear resistance between the fibre and matrix, therefore, higher resistance results in stiffer response of the composites as illustrated in Fig. 6. Another aspect of Fig. 6 is that there is an increasing difference in the composites modulus with different volume fraction but the same interfacial stiffness. For instance, for the interfacial stiffness of 15GPa, the gap between volume fraction of 35% and 50% is about 5GPa, while the gap increases to about 13GPa for the interfacial stiffness of 30GPa. This implies that for the same interfacial stiffness, the interfacial resistance is higher for composites of higher fibre volume fraction Fig. 6 conveys the significance that the cohesive interface plays a more important role in the composites with higher fibre volume fraction. This is because the total area of the cohesive interface is larger when the fibre volume fraction is bigger while other aspects are kept the same.

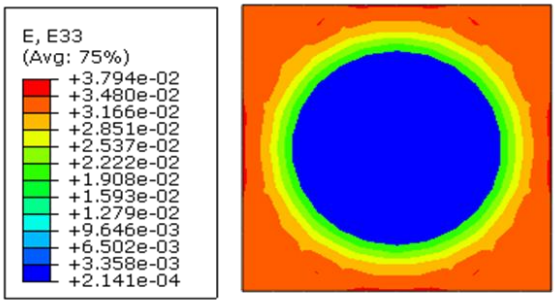

Figure 5 Strain contour at loading end of the composites (35% fibre volume fraction)

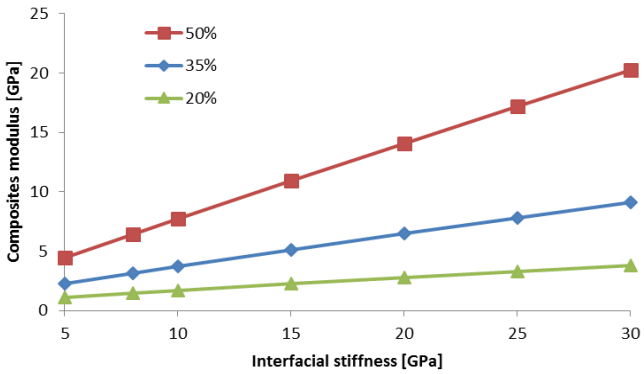

Figure 6 Axial moduli of composites with different fibre volume fraction against interfacial stiffness

4 CONCLUSIONS

The mechanical properties of the bio-compatible and fully bio-resorbable glass fibre reinforced composites were investigated by the FE model. The FE model assumed that the interface between the fibre and the matrix was represented by a layer of cohesive elements. It was shown that this FE model was capable to model the performance of the composites with fibre volume fractions and interfacial stiffness.

The void ratio of the composites was captured and evaluated by taking SEM images and processed by image analysis technique. The influence of the void ratio was integrated into the interfacial modulus. It was shown that the void ratio had negative influence on the mechanical properties of the composites. According to the FE results, the variation of the interfacial modulus influenced the performance of the composites significantly. It was also found that the elastic modulus of the composites increased steadily as the interfacial modulus increased.

The FE model demonstrated the capability of modelling the performance of composites with various fibre volume fractions, particularly for high fibre volume fraction. For the mediate and low fibre volume fraction, the influence of the cohesive interface can still be observed, however, less significantly than high fibre volume fraction

ACKNOWLEDGEMENTS

The author gratefully acknowledges the scholarship granted by International Doctoral Innovation Centre (IDIC), University of Nottingham Ningbo China.

REFERENCES

1. Engh, C.A., J. Bobyn, and A.H. Glassman, *Porous-coated hip replacement. The factors governing bone ingrowth, stress shielding, and clinical results.* Bone & Joint Journal, 1987. **69**(1): p. 45-55.
2. Huiskes, R., H. Weinans, and B. Van Rietbergen, *The relationship between stress shielding and bone resorption around total hip stems and the effects of flexible materials.* Clinical orthopaedics and related research, 1992. **274**: p. 124-134.
3. Nagels, J., M. Stokdijk, and P.M. Rozing, *Stress shielding and bone resorption in shoulder arthroplasty.* Journal of shoulder and elbow surgery, 2003. **12**(1): p. 35-39.

4. Parsons, A.J., et al., *Phosphate Glass Fibre Composites for Bone Repair.* Journal of Bionic Engineering, 2009. **6**(4): p. 318-323.
5. Törmälä, P., T. Pohjonen, and P. Rokkanen, *Bioabsorbable polymers: materials technology and surgical applications.* Proceedings of the Institution of Mechanical Engineers, Part H: Journal of Engineering in Medicine, 1998. **212**(2): p. 101-111.
6. Hoffmann, J., et al., *A totally bioresorbable fibrillar reinforced composite system: structure and properties.* International Journal of Polymeric Materials, 2001. **50**(3-4): p. 469-482.
7. Chen, M., et al., *In-situ polymerisation of fully bioresorbable polycaprolactone/phosphate glass fibre composites: In vitro degradation and mechanical properties.* Journal of the Mechanical Behavior of Biomedical Materials, 2016. **59**: p. 78-89.
8. Wambua, P., J. Ivens, and I. Verpoest, *Natural fibres: can they replace glass in fibre reinforced plastics?* composites science and technology, 2003. **63**(9): p. 1259-1264.
9. Taj, S., M.A. Munawar, and S. Khan, *Natural fiber-reinforced polymer composites.* Proceedings-Pakistan Academy of Sciences, 2007. **44**(2): p. 129.
10. Bitar, M., et al., *Soluble phosphate glasses: in vitro studies using human cells of hard and soft tissue origin.* Biomaterials, 2004. **25**(12): p. 2283-2292.
11. Parsons, A., et al., *Synthesis and degradation of sodium iron phosphate glasses and their in vitro cell response.* Journal of Biomedical Materials Research Part A, 2004. **71**(2): p. 283-291.
12. Imai, Y., M. Nagai, and M. Watanabe, *Degradation of composite materials composed of tricalcium phosphate and a new type of block polyester containing a poly (L-lactic acid) segment.* Journal of Biomaterials Science, Polymer Edition, 1999. **10**(4): p. 421-432.
13. Ramakrishna, S., et al., *Biomedical applications of polymer-composite materials: a review.* Composites science and technology, 2001. **61**(9): p. 1189-1224.
14. Mano, J.F., et al., *Bioinert, biodegradable and injectable polymeric matrix composites for hard tissue replacement: state of the art and recent developments.* Composites Science and Technology, 2004. **64**(6): p. 789-817.
15. Ahmed, I., et al., *Retention of mechanical properties and cytocompatibility of a phosphate‐based glass fiber/polylactic acid composite.* Journal of Biomedical Materials Research Part B: Applied Biomaterials, 2009. **89**(1): p. 18-27.
16. Felfel, R., et al., *In vitro degradation, flexural, compressive and shear properties of fully bioresorbable composite rods.* Journal of the mechanical behavior of biomedical materials, 2011. **4**(7): p. 1462-1472.
17. Furukawa, T., et al., *Biodegradation behavior of ultra-high-strength hydroxyapatite/poly (L-lactide) composite rods for internal fixation of bone fractures.* Biomaterials, 2000. **21**(9): p. 889-898.
18. Li, V.C. and H. Stang, *Interface property characterization and strengthening mechanisms in fiber reinforced cement based composites.* Advanced Cement Based Materials, 1997. **6**(1): p. 1-20.
19. Kang, G.-Z. and Q. Gao, *Tensile properties of randomly oriented short δ-Al2O3 fiber reinforced aluminum alloy composites: II. Finite element analysis for stress transfer, elastic modulus and stress–strain curve.* Composites Part A: Applied Science and Manufacturing, 2002. **33**(5): p. 657-667.
20. DiFrancia, C., T.C. Ward, and R.O. Claus, *The single-fibre pull-out test. 1: Review and interpretation.* Composites Part A: Applied Science and Manufacturing, 1996. **27**(8): p. 597-612.

21. Budiman, B.A., et al., *Evaluation of interfacial strength between fiber and matrix based on cohesive zone modeling.* Composites Part A: Applied Science and Manufacturing, 2016. **90**: p. 211-217.
22. Soni, G., et al., *Modelling matrix damage and fibre–matrix interfacial decohesion in composite laminates via a multi-fibre multi-layer representative volume element (M2RVE).* International Journal of Solids and Structures, 2014. **51**(2): p. 449-461.
23. Maligno, A.R., *Finite element investigations on the microstructure of composite materials*. 2008, University of Nottingham.
24. Sun, C.T. and R.S. Vaidya, *Prediction of composite properties from a representative volume element.* Composites Science and Technology, 1996. **56**(2): p. 171-179.
25. Huang, Z.-M., *Simulation of the mechanical properties of fibrous composites by the bridging micromechanics model.* Composites Part A: Applied Science and Manufacturing, 2001. **32**(2): p. 143-172.
26. Madsen, B. and H. Lilholt, *Physical and mechanical properties of unidirectional plant fibre composites—an evaluation of the influence of porosity.* Composites Science and Technology, 2003. **63**(9): p. 1265-1272.
27. Barbero, E.J., *Finite element analysis of composite materials using AbaqusTM*. 2013: CRC press.
28. Manual, A.U., *Version 6.10.* ABAQUS Inc, 2010.
29. Guo, H., et al., *Interface property of carbon fibers/epoxy resin composite improved by hydrogen peroxide in supercritical water.* Materials Letters, 2009. **63**(17): p. 1531-1534.
30. Jia, Y., W. Yan, and H.-Y. Liu. *Numerical study on carbon fibre pullout using a cohesive zone model*.
31. Chambers, A.R., et al., *The effect of voids on the flexural fatigue performance of unidirectional carbon fibre composites developed for wind turbine applications.* International Journal of Fatigue, 2006. **28**(10): p. 1389-1398.